Letter

Toward a neutrino-limited dark matter search with crystalline xenon

Hao Chen,[1,*] Ryan Gibbons,[1,2] S. J. Haselschwardt,[1] Scott Kravitz,[3] Qing Xia,[1] and Peter Sorensen[1,†]

[1]*Lawrence Berkeley National Laboratory, 1 Cyclotron Road, Berkeley, California 94720, USA*
[2]*Department of Physics, University of California, Berkeley, Berkeley, California 94720, USA*
[3]*Department of Physics, The University of Texas at Austin, 2515 Speedway, Austin, Texas 78712, USA*

(Received 22 December 2023; accepted 4 April 2024; published 29 April 2024)

Experiments searching for weakly interacting massive particle dark matter are now detecting background events from solar neutrino-electron scattering. However, the dominant radioactive background in state-of-the-art experiments such as LZ and XENONnT is beta decays from radon contamination. In spite of careful detector material screening, radon progenitor atoms are ubiquitous and long-lived, and radon is extremely soluble in liquid xenon. We propose a change of phase and demonstrate that crystalline xenon offers more than a factor ×500 exclusion against radon ingress, compared with the liquid state. This level of radon exclusion would allow crystallized versions of existing experiments to probe spin-independent cross sections near 10^{-47} cm^2 in roughly 11 years, as opposed to the 35 years required otherwise.

DOI: 10.1103/PhysRevD.109.L071102

Introduction. Astrophysical observations and cosmological models suggest that 84% of the total matter density in the Universe is nonluminous, nonbaryonic dark matter [1,2]. The majority, if not all, of the dark matter requires new particles beyond the Standard Model [3]. For decades, the most well-motivated class of models has been the weakly interacting massive particle (WIMP) [4]. Significant experimental effort has been dedicated to detecting WIMP-nucleon interactions [5], but unambiguous evidence has yet to be observed [6].

Currently, the most sensitive exclusion limits on the interaction cross section for WIMPs with masses greater than about 10 GeV are due to the LUX-ZEPLIN (LZ) experiment [7], which utilizes a 7 tonne active target composed of a liquid xenon time projection chamber (TPC). The LZ experiment attempts to detect WIMPs by searching for nuclear recoil events at the keV energy scale, and the background rate in the approximately 1–10 keV energy range of interest for WIMP scattering is < 1 mHz/kg/day [8]. About 1/10 of these events are due to irreducible solar neutrino-electron scattering. Eventually, it is hoped that this class of experiments will reach a sensitivity that is limited by coherent neutrino-nucleus scattering of solar and atmospheric neutrinos [5], which is variously referred to as the neutrino detection limit, the neutrino floor, or the neutrino fog [9]. However, progress toward this goal is obscured by the fact that at present, some 2/3 of the observed background events are due to ground-state beta decays of ^{214}Pb and ^{212}Pb, from the decay of ^{222}Rn and ^{220}Rn [7].

Radon is typically present at ppm levels [10] and emanates from a wide range of materials. It is soluble in liquids, including liquid xenon. Material screening prior to detector construction is essential but not sufficient. LZ employs a charcoal chromatography radon reduction system [11] in the vapor phase for on-line purification, and achieved a ^{222}Rn concentration of 3.26 μBq/kg. XENONnT [12,13] achieved a significantly lower ^{222}Rn concentration of 0.8 μBq/kg background using an in-line cryogenic distillation column [14]. These techniques compete against continuous emanation of radon from detector materials, so the efficacy scales with the xenon circulation rate.

We previously demonstrated [15] that crystalline and liquid xenon have nearly identical scintillation yields and similar ionization yields. The factor of about ×2 higher electron mobility in crystalline xenon [16] is an additional benefit for the suppression of pileup. Ionized electrons are emitted from crystalline xenon with 60% greater efficiency, compared with liquid xenon [17]. In this Letter, we demonstrate the key motivation for this technology: crystalline xenon's ability to exclude radon contamination. The effect on future dark matter searches is quantified.

Radon exclusion from crystalline xenon. In order to quantify the transport of radon into the condensed state, we exposed a small dual-phase xenon TPC [15] to an $\mathcal{O}(1)$ Hz source of ^{222}Rn ($t_{1/2} = 3.8$ days), and an

*maque@lbl.gov
†pfsorensen@lbl.gov

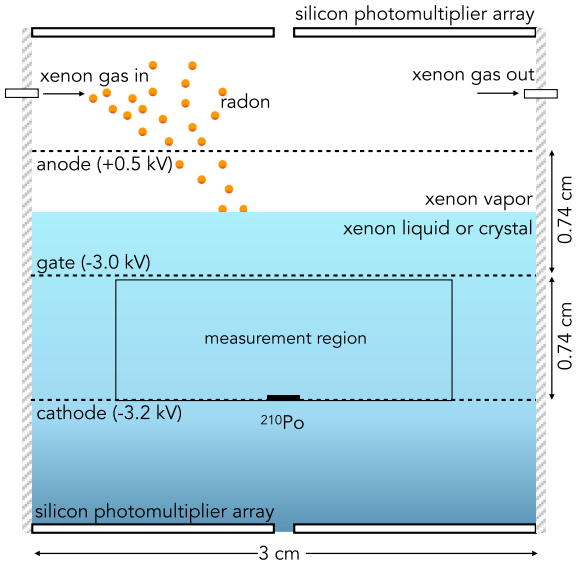

FIG. 1. Schematic of the experimental apparatus, approximately to scale. Radon atoms (indicated) were introduced via the sealed xenon gas circulation loop.

$\mathcal{O}(100)$ Hz source of ^{220}Rn ($t_{1/2} = 56$ seconds), and measured the resulting number of alpha particles from their decay. The radon was introduced into the vapor phase via a sealed xenon circulation and purification system.

Instrument: The cylindrical TPC is made of polytetrafluoroethylene with an internal radius of 1.5 cm, as shown in Fig. 1. Three mesh electrodes (cathode, gate, and anode) with 7.4 mm spacing define the electric fields. The TPC was operated with the cathode at −3.2 kV, the gate at −3.0 kV and the anode at +0.5 kV. Xenon was purified using a SAES PS3 getter. The liquid/vapor (or crystal/vapor) interface was about half way between the gate and the anode.[1]

Particle interactions generate both prompt scintillation photons (referred to as S1) and ionization signals (referred to as S2). The ionized electrons are drifted across the liquid/crystal by an electric field $E = 270$ V/cm applied between the cathode and the gate electrode, then emitted into the vapor phase above by a stronger electric field of approximately $E = 3000$ V/cm between the gate and anode. Acceleration of the electrons through the vapor produces an electroluminescence signal proportional to the number of electrons (the S2 signal). The time difference between the S1 and S2 signals corresponds to the z coordinate of the interaction. The photon distribution of the S2 signal gives the (x, y) coordinates. Two 16-channel arrays of silicon photomultiupliers (Hamamatsu S13371-6050CQ) above and below the measurement region detect the 175 nm photons. We note that each silicon photomultiplier channel contains 13,923 individual single-photon sensitive pixels. Signal saturation is about 7% for S2 $= 10^{4.5}$ phd. This leads to a slight nonlinearity of the reconstructed alpha energies, but does not affect the measurements.

A ^{210}Po alpha particle calibration source was deposited in the center of the cathode mesh. The source emits 5.3 MeV alphas which are less energetic than the alpha decays we need to count. For the data reported in Sec. II B, the source was deposited on a 3 mm diameter integrated disk. The disk lead to additional dispersion in the S1 and S2 signals, so for subsequent data (Sec. II C) we removed the disk and deposited the source directly on the cathode mesh. This lead to larger S1 signals and a wider dispersion of the source response, due to the trajectories of alpha particles with respect to the mesh. In both cases, the bulk radon alpha population is easy to identify by the deposited energy and the location of events. We used the alpha rates and light yield from ^{210}Po in liquid/vapor mode and crystal/vapor mode to confirm that the detector had similar detection efficiency for MeV alphas in each of the two operation modes. Upon liquefaction and again upon crystallization, we measured the light yield from 122 and 136 keV (^{57}Co) gammas and found these to be similar to within a few percent. The electron lifetime was $\tau = 183 \pm 7$ μs in the liquid and crystal data during the ^{222}Rn test, and $\tau = 314 \pm 17$ μs during the ^{220}Rn test, leading to at most a 13% variation in S2.

To avoid nonuniformity of the applied electric fields, single scatter events were required to occur within a radius $r < 1$ cm. Events in the 3–4 mm of xenon liquid or crystal above the gate electrode were excluded since the S1 and S2 signals can overlap. Events in the vapor are mostly rejected based on their time profile and/or by a reduced S2 size. An example of data satisfying the selection criteria is shown in Fig. 2. Beta and gamma background events are well-separated from the alpha populations. Note that data were analyzed and are presented without (x, y, z) corrections, aside from reconstructed energy spectra. This choice leads to a strong separation between the ^{210}Po calibration alphas from the radon source alphas, due to cathode shadowing.

An $n \geq 2$ coincidence threshold trigger had full efficiency for alpha particle events. The TPC was enclosed in 5 cm of lead bricks, and the total background trigger rate was about 7 Hz. The highest trigger rate for data described here was less than 20 Hz.

Radon exclusion measurement with ^{222}Rn: A SAES GPU IX purifier was found to provide a flow-through source of ^{222}Rn. It was installed in addition to the PS3 getter. Xenon gas was circulated continuously at a fixed flow rate of 0.3 ± 0.01 standard liters per minute in order to fix the rate of introduction of ^{222}Rn atoms.

In addition to the 5.5 MeV alpha from ^{222}Rn, early progeny ^{218}Po emits a 6.0 MeV alpha and ^{214}Po emits a

[1]The interface height was slightly different in each case due to the change in density, which can lead to a variation of about 20% in the S2 signal size.

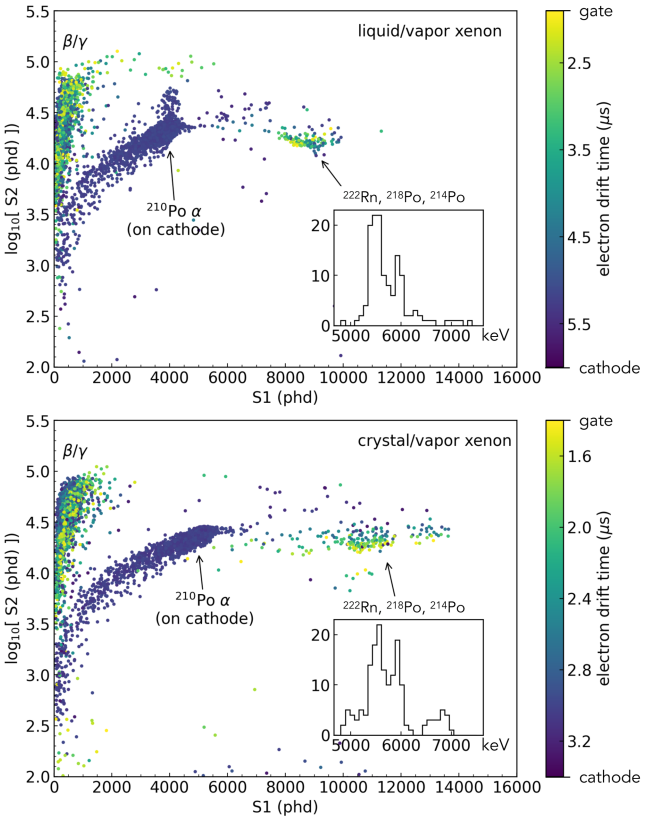

FIG. 2. Top: distribution of scintillation (S1) and ionization (S2) signals from single scatter events in the measurement region, after circulating ^{222}Rn in liquid/vapor mode for 210 hours. Bottom: the same distribution in crystal/vapor mode, about 45 hours after crystallizing. Inset plots show the reconstructed energy spectra of the bulk radon events. The population of events with S2 ∼ 200 phd are due to ^{210}Po source decays at the edges of the disk.

7.7 MeV alpha. The problematic dark matter search background from beta decay of ^{214}Pb is bracketed by these polonium decays. Due to the finite energy resolution of the instrument, we do not attempt to distinguish the alpha particles by energy, and instead count all of them as an ensemble. This leads to a slight underestimate in the deduced radon exclusion factor, because we observe less ^{214}Po in the liquid phase: it often drifts to the cathode before it decays, whereas in the crystal phase it cannot do so.

The purifier radon source was operated continuously, and the rate of alpha particles was recorded for nearly one month, as shown in Fig. 3. The instrument was in liquid/vapor mode at a vapor pressure p ≈ 1.25 Bar for the first nine days. The slow increase in the alpha count rate in proportion to $1 - e^{-\lambda t}$ over the first nine days reflects the approach to secular equilibrium of the ^{222}Rn rate. Here, $\lambda = \log(2)/t_{1/2}$ and $t_{1/2} = 92$ hours.

Over a period of about four days, the xenon was crystallized. Data were not acquired during this time, because the crystallization procedure requires filling additional liquid xenon above the anode. The count rate of alpha particles in crystal/vapor mode at a vapor pressure p ≈ 0.79 Bar was then observed for about thirteen days. The alpha particle rate decreased exponentially following the half life of ^{222}Rn. We conclude that these atoms were trapped in the condensed state during crystallization, and no new radon atoms were able to diffuse into the crystal.

The offset between the extrapolation of liquid phase alpha counts shown in Fig. 3 and the start of crystal alpha counts is due to the decay of polonium daughters: half of the ^{218}Po and 76% of ^{214}Bi are left with net positive charge [18] and in liquid can drift to the cathode where in this experiment we would not count them. In the crystalline state, the daughters are frozen in the crystal matrix and so are always counted.

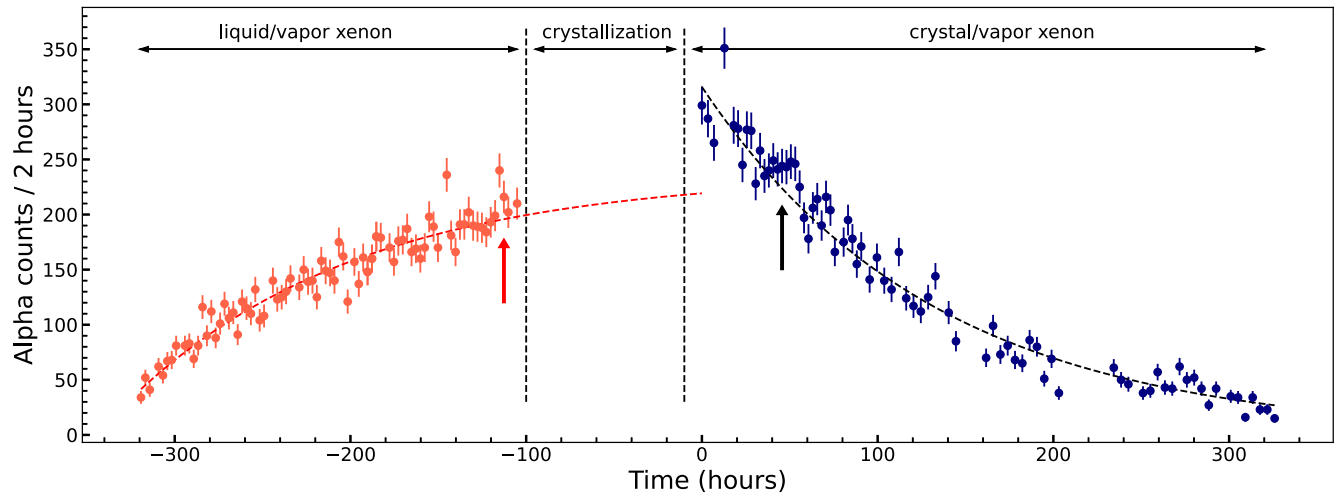

FIG. 3. Count rate of alpha decays in the measurement region during continuous introduction of ^{222}Rn. The count rate initially increased in proportion to $1 - e^{-\lambda t}$, with $\lambda = \log(2)/t_{1/2}$ and $t_{1/2} = 92$ hours. In crystal/vapor mode the count rate decreased as $e^{-\lambda t}$, indicating that no new radon could enter the crystal. Arrows indicate the two data sets shown in Fig. 2.

Extrapolation of the liquid phase count rate trend to $t = 320$ hours suggests that we would have observed about 240 counts per two hours had we not crystallized the xenon. Given the observation of about 20 counts per two hours, crystallization reduces the radon ingress by a factor of $\times 12$. It turns out this is a significant underestimate.

Radon exclusion measurement with ^{220}Rn: We repeated the test procedure with a higher-activity ^{220}Rn source from Pylon Electronics instead of the SAES GPU IX source. In addition to the 6.3 MeV alpha from ^{220}Rn, its early progeny ^{216}Po also emits an alpha particle with energy 6.8 MeV. Data sets were started 10 minutes after initiating the radon flow, at which point the radon event rate $1 - e^{-\lambda t}$ had saturated due to $\lambda = 0.756$ min^{-1}.

Given the half life of ^{220}Rn, we expected to count zero events from ^{220}Rn alpha decay in crystal/vapor mode. The signal distributions are shown in Fig. 4. Four hour data sets recorded 2034 alpha events in the measurement region in liquid/vapor mode, compared with three events in the crystal/vapor mode. All three observed alpha events are nearly in the center of the crystal based on the electron drift time. Two of the three events appear to be due to ^{222}Rn followed by ^{218}Po, accidentally trapped during the crystallization process. They occurred at the same reconstructed (x, y, z) location in the crystal (within the resolution of the instrument), and with a time delay very close to the 3.1 minute half life of ^{218}Po.

We therefore consider the 90% confidence level Poisson upper limit on one observed event ($n = 3.9$) and obtain a radon exclusion factor of more than $\times 500$ at 90% CL for crystalline xenon with respect to liquid xenon. We suspect that this factor is a lower limit, but data acquisition rate limitations preclude us from testing a higher radon activity. We also note that if we were to count all three events as ingress of ^{220}Rn, the 90% confidence level Poisson upper limit would be $n = 6.7$, and the reduction factor would be closer to $\times 300$. This would still be more than sufficient to render radon irrelevant as a background for the projections we make in the next section.

Discussion. We measured radon transport efficiency across a xenon vapor/liquid interface relative to a xenon vapor/crystal interface. We assume a similar factor would apply to other materials m_x used for detector construction, since it is the interaction of a radon atom with an atom of the condensed state (either liquid or crystal) which is relevant. In other words, we assume the measured exclusion factor also applies to radon transport across m_x/liquid xenon vs m_x/crystal xenon interfaces. Similar studies of radon interaction with liquid and crystal water support this view [19].

During its first science run, the LZ experiment observed 182 background events from beta decays of ^{214}Pb and ^{212}Pb from the ^{222}Rn and ^{220}Rn chains, respectively [8]. Our work suggests that if it had been able to operate in crystal/vapor mode with all other factors equal, this could have been reduced to < 1 background event.

In order to quantify the potential benefit of a radon-free crystalline/vapor xenon TPC, we compare the projected sensitivity of an LZ-like experiment with and without radon. We assume here that the detection threshold, discrimination, and photon and electron yields of the crystal phase are identical to those in liquid. We use as a baseline the projected background rate of 6.2 counts in 1000 days from Ref. [20]. This rate was estimated in the energy range of 6–30 keV for nuclear recoil signals, after 99.5% discrimination of electron recoils from nuclear recoils. We also assume effectively all of the radioactive krypton could be removed by, e.g., charcoal chromatography [21] or cryogenic distillation [22], which is justified by existing technology. This leaves an expected background rate after discrimination of 2 counts in 1000 days. This rate is dominated by solar neutrino scattering from atomic electrons, followed by two-neutrino double beta decay of ^{136}Xe. The expected background rate for the same volume of a crystal/vapor LZ-like instrument (colloquially: "CrystaLiZe") would be 20% larger due to the

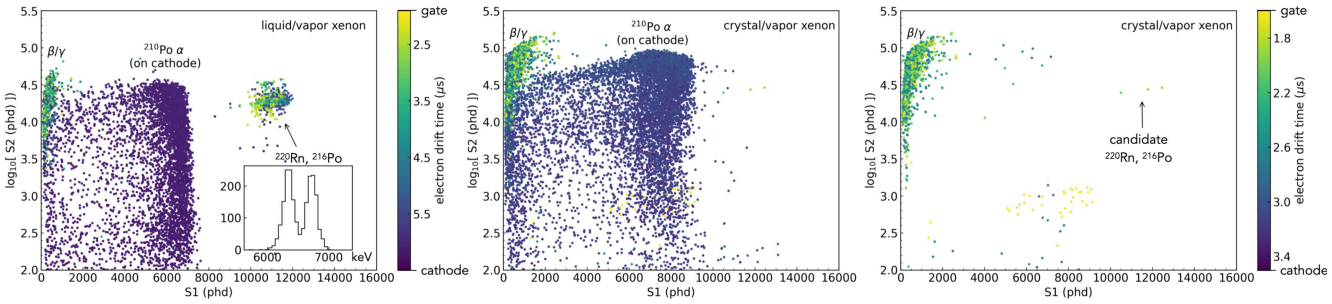

FIG. 4. Left: distribution of scintillation (S1) and ionization (S2) signals from single scatter events in the measurement region during four hours of continuously circulating ^{220}Rn in liquid/vapor mode. Center: the same distributions obtained during four hours of continuously circulating ^{220}Rn in crystal/vapor mode. Right: same as center, but with cathode events removed for clarity. Three candidate alpha events in the crystal are observed. The population with S2 $\sim$ 1000 is due to radon decays in the vapor above the anode (short electron drift times) and to the tail of ^{210}Po source decays (long electron drift times).

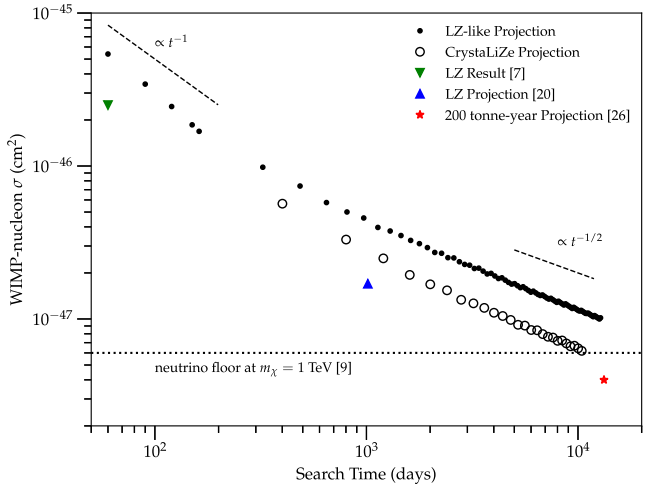

FIG. 5. The projected sensitivity of an LZ-like detector to spin-independent scattering of 1 TeV dark matter particles, in the case of either 5.5 tonne active liquid xenon mass (filled circles) or 6.6 tonne active crystal xenon mass (open circles). Also shown are the recent LZ first results [7], LZ projection [20], and projected sensitivity of a 200 tonne-year exposure of a next generation experiment [26] scaled to a 5.5 tonne target.

change in density. We assume the same discrimination of 99.5% against electron recoils and 50% nuclear recoil acceptance in both liquid and crystalline xenon, as in [20].

In Fig. 5, we show how the sensitivity to the spin-independent WIMP-nucleon cross section for hypothetical WIMP mass of 1 TeV improves as a function of search time. This mass was chosen for its evasion of collider constraints on simplified dark matter models [23] and in light of a suite of electroweak benchmark candidates [24] lying above 1 TeV. A Feldman-Cousins "cut-and-count" method [25] was used in both cases. The difference is significant: in order to reach a sensitivity of $\sigma = 1 \times 10^{-47}$ cm^2, a radon-free crystalline xenon instrument would require about 4000 live days (11 years), a factor $\times 3$ less search time than the 12,700 live days (35 years) required otherwise. The former time period is likely comparable to the construction time for a next-generation instrument [26], while the latter is comparable to the duration of any one researcher's career. The cross section benchmark $\sigma = 1 \times 10^{-47}$ cm^2 lies just above the neutrino "floor" as defined in Ref. [9]. The sensitivity projection for crystalline xenon should also apply to a liquid xenon instrument with significantly improved radon reduction.

Liquid xenon instruments have also been used for other new physics searches beyond WIMP dark matter. One example is axionlike particle and hidden photon models, or searches for a neutrino magnetic moment [27,28]. In these cases, the expected signal is an electron recoil in a xenon TPC. Since these would look similar to the low-energy beta background from radon, a crystalline xenon TPC would be even more beneficial to such searches. Additionally, a proposal to dope a light element such as hydrogen or helium into a large liquid xenon TPC (HydroX) in order to increase sensitivity to low-mass dark matter [29,30] could possibly be improved by using crystalline xenon. This is because two key concerns for HydroX are (1) that light elements could diffuse through the seal on the photomultiplier tubes, leading to their rapid aging, and (2) hydrogen would dominate the vapor phase and would quench the S2 signal. If the light element were frozen in a crystal, the hydrogen-rich vapor could be pumped off and replaced with pure xenon. Finally, experiments searching for the zero-neutrino mode of double beta decay in the isotope ^{136}Xe could possibly benefit by considering crystalline xenon in the context of barium tagging [31].

Conclusion. A crystal/vapor dual-phase TPC appears to be a promising detector technology for reaching the dark matter neutrino detection limit in a reasonable time scale utilizing existing experimental infrastructure. If it proves feasible to crystallize the LZ experiment or the XENONnT experiment following conclusion of their science goals, either of these $\mathcal{O}(10)$ tonne xenon target instruments could optimistically reach $\sigma = 1 \times 10^{-47}$ cm^2 in 11 years of search time. A previous scalability study [32] suggests the crystallization process may take a year for an instrument of this size. More R&D is needed: (a) the scaling to tens or hundreds of kilograms of target mass must be demonstrated, (b) calibration strategies need to be tested, (c) the crystal quality, surface, and presence of impurities at such a scale needs to be quantified, (d) the incident particle type discrimination of a crystal/vapor xenon TPC needs to be measured, and (e) the stability over long time periods needs to be assessed.

Acknowledgments. A. Manalaysay provided advice on the Feldman-Cousins sensitivity projections. We are grateful to the referees for catching an error in an earlier manuscript. This material is based upon work supported by the U.S. Department of Energy, Office of Science, Office of High Energy Physics, under Award No. DE-AC02-05CH1123.

[1] N. Aghanim *et al.* (Planck Collaboration), Planck 2018 results. VI. Cosmological parameters, Astron. Astrophys. **641**, A6 (2020); **652**, C4(E) (2021).

[2] Y. Sofue and V. Rubin, Rotation curves of spiral galaxies, Annu. Rev. Astron. Astrophys. **39**, 137 (2001).

[3] R. L. Workman *et al.* (Particle Data Group), Review of particle physics, Prog. Theor. Exp. Phys. **2022**, 083C01 (2022).

[4] L. Baudis, Direct dark matter detection: The next decade, Phys. Dark Universe **1**, 94 (2012). Next Decade in Dark Matter and Dark Energy.

[5] D. S. Akerib *et al.*, Snowmass2021 cosmic frontier dark matter direct detection to the neutrino fog, in *Snowmass 2021* (2022), arXiv:2203.08084.

[6] M. Schumann, Direct detection of WIMP dark matter: Concepts and status, J. Phys. G **46**, 103003 (2019).

[7] J. Aalbers *et al.* (LUX-ZEPLIN Collaboration), First dark matter search results from the LUX-ZEPLIN (LZ) experiment, Phys. Rev. Lett. **131**, 041002 (2023).

[8] J. Aalbers *et al.* (LUX-ZEPLIN Collaboration), Background determination for the LUX-ZEPLIN dark matter experiment, Phys. Rev. D **108**, 012010 (2023).

[9] C. A. J. O'Hare, New definition of the neutrino floor for direct dark matter searches, Phys. Rev. Lett. **127**, 251802 (2021).

[10] J. A. Formaggio and C. J. Martoff, Backgrounds to sensitive experiments underground, Annu. Rev. Nucl. Part. Sci. **54**, 361 (2004).

[11] D. S. Akerib *et al.* (LZ Collaboration), The LUX-ZEPLIN (LZ) radioactivity and cleanliness control programs, Eur. Phys. J. C **80**, 1044 (2020); **82**, 221(E) (2022).

[12] E. Aprile *et al.* (XENON Collaboration), First dark matter search with nuclear recoils from the XENONnT experiment, Phys. Rev. Lett. **131**, 041003 (2023).

[13] D. Koke *et al.* (XENON Collaboration), The XENONnT radon removal system, in *XVIII International Conference on Topics in Astroparticle and Underground Physics (TAUP 2023)* (2023), https://indico.cern.ch/event/1199289/contributions/5449603/attachments/2703010/4691861/Radon%20TAUP%20Poster%20v4.pdf.

[14] M. Murra, D. Schulte, C. Huhmann, and C. Weinheimer, Design, construction and commissioning of a high-flow radon removal system for XENONnT, Eur. Phys. J. C **82**, 1104 (2022).

[15] S. Kravitz, H. Chen, R. Gibbons, S. J. Haselschwardt, Q. Xia, and P. Sorensen, Operation and performance of a dual-phase crystalline/vapor xenon time projection chamber, J. Instrum. **17**, P04014 (2022).

[16] U. Asaf and I. T. Steinberger, Photoconductivity and electron transport parameters in liquid and solid xenon, Phys. Rev. B **10**, 4464 (1974).

[17] E. M. Gushchin, A. A. Kruglov, and I. M. Obodovskil, Emission of "hot" electrons from liquid and solid argon and xenon, J. Exp. Theor. Phys. **55**, 860 (1982).

[18] J. B. Albert *et al.* (EXO-200 Collaboration), Measurements of the ion fraction and mobility of α- and β-decay products in liquid xenon using the EXO-200 detector, Phys. Rev. C **92**, 045504 (2015).

[19] B. Eichler, H. P. Zimmerman, and H. W. Gaggeler, Adsorption of radon on ice surfaces, J. Phys. Chem. A **104**, 3126 (2000).

[20] D. S. Akerib *et al.* (LZ Collaboration), Projected WIMP sensitivity of the LUX-ZEPLIN dark matter experiment, Phys. Rev. D **101**, 052002 (2020).

[21] A. Ames (LUX-ZEPLIN Collaboration), Krypton removal via gas chromatography for the LZ experiment, AIP Conf. Proc. **2908**, 070001 (2023).

[22] E. Aprile *et al.* (XENON Collaboration), Removing krypton from xenon by cryogenic distillation to the ppq level, Eur. Phys. J. C **77**, 275 (2017).

[23] G. Aad *et al.* (ATLAS Collaboration), Search for supersymmetry in final states with jets, missing transverse momentum and one isolated lepton in $\sqrt{s} = 7$ TeV pp collisions using 1 fb^{-1} of ATLAS data, Phys. Rev. D **85**, 012006 (2012); **87**, 099903(E) (2013).

[24] S. Bottaro, D. Buttazzo, M. Costa, R. Franceschini, P. Panci, D. Redigolo, and L. Vittorio, Closing the window on WIMP dark matter, Eur. Phys. J. C **82**, 31 (2022).

[25] G. J. Feldman and R. D. Cousins, A unified approach to the classical statistical analysis of small signals, Phys. Rev. D **57**, 3873 (1998).

[26] J. Aalbers *et al.*, A next-generation liquid xenon observatory for dark matter and neutrino physics, J. Phys. G **50**, 013001 (2023).

[27] E. Aprile *et al.* (XENON Collaboration), Search for new physics in electronic recoil data from XENONnT, Phys. Rev. Lett. **129**, 161805 (2022).

[28] J. Aalbers *et al.* (LZ Collaboration), Search for new physics in low-energy electron recoils from the first LZ exposure, Phys. Rev. D **108**, 072006 (2023).

[29] H. Lippincott, T. Alexander, and A. Hime, Increasing the sensitivity of LXe TPCs to dark matter by doping with helium or neon, Proc. Sci. ICHEP2016 (**2017**) 285.

[30] S. J. Haselschwardt, R. Gibbons, H. Chen, S. Kravitz, A. Manalaysay, Q. Xia, P. Sorensen, and W. H. Lippincott, First measurement of discrimination between helium and electron recoils in liquid xenon for low-mass dark matter searches, Phys. Rev. Lett. **132**, 111801 (2024).

[31] nEXO Collaboration, Imaging individual barium atoms in solid xenon for barium tagging in nEXO, Nature (London) **569**, 203 (2019).

[32] J. Yoo, H. Cease, W. F. Jaskierny, D. Markley, R. B. Pahlka, D. Balakishiyeva, T. Saab, and M. Filipenko, Scalability study of solid xenon, J. Instrum. **10**, P04009 (2015).